



UNIVERSITÀ DI PARMA

ARCHIVIO DELLA RICERCA

University of Parma Research Repository

Anti-proliferative effects of copper(II) complexes with hydroxyquinoline-thiosemicarbazone ligands

This is the peer reviewed version of the following article:

Original

Anti-proliferative effects of copper(II) complexes with hydroxyquinoline-thiosemicarbazone ligands / Rogolino, Dominga; Cavazzoni, Andrea; Gatti, Anna; Tegoni, Matteo; Pelosi, Giorgio; Verdolino, Vincenzo; Fumarola, Claudia; Cretella, Daniele; Petronini, Pier Giorgio; Carcelli, Mauro. - In: EUROPEAN JOURNAL OF MEDICINAL CHEMISTRY. - ISSN 0223-5234. - 128:(2017), pp. 140-153. [10.1016/j.ejmech.2017.01.031]

Availability:

This version is available at: 11381/2822139 since: 2023-07-08T20:17:12Z

Publisher:

Elsevier Masson s.r.l.

Published

DOI:10.1016/j.ejmech.2017.01.031

Terms of use:

Anyone can freely access the full text of works made available as "Open Access". Works made available

Publisher copyright

note finali coverpage

(Article begins on next page)

Anti-proliferative Effects of Copper(II) Complexes with Hydroxyquinoline-Thiosemicarbazone Ligands

Dominga Rogolino^{±*}, Andrea Cavazzoni^{§§}, Anna Gatti[±], Matteo Tegoni[±], Giorgio Pelosi[±], Vincenzo Verdolino^{†‡}, Claudia Fumarola[§], Daniele Cretella[§], Pier Giorgio Petronini[§], Mauro Carcelli[±]

[±]*Dipartimento di Chimica and Consorzio Interuniversitario di Ricerca in Chimica dei Metalli nei Sistemi Biologici, Università di Parma, Parco Area delle Scienze 17/A, 43124 Parma, Italy*

[§]*Department of Clinical and Experimental Medicine, University of Parma*

[†]*Department of Chemistry and Applied Biosciences, Eidgenössische Technische Hochschule Zürich, CH-8093 Zurich, Zurich, Switzerland*

[‡]*Facoltà di Informatica, Istituto di Scienze Computazionali, Università della Svizzera Italiana, 6900 Lugano, Ticino, Switzerland*

* corresponding author

Prof. Dominga Rogolino

Dipartimento di Chimica and Consorzio Interuniversitario di Ricerca in Chimica dei Metalli nei Sistemi Biologici, Università di Parma

Parco Area delle Scienze 17/A, 43124 Parma, Italy

dominga.rogolino@unipr.it

+39 0521 905419

[§] Co-corresponding author: authors equally contributed to the present work

ABSTRACT

The possibility to influence the physiological concentration of copper ions through the careful choice of ligands is emerging as a novel intriguing strategy in the treatment of pathologies such as cancer and Alzheimer. Thiosemicarbazones play an important role in this field, because they offer a wide variety of potential functionalizations and different kinds of coordination modes. Here we report the synthesis of some 8-hydroxyquinoline thiosemicarbazone ligands containing an ONN'S donor set and their Zn(II) and Cu(II) complexes. The metal complexes are characterized in solution and in the solid state and the X-ray structure of one of the copper(II) complex is reported. The Cu(II) complexes were characterized also by means of quantum mechanical calculations. The Cu(II) complexes displayed cytostatic activity in different cancer cell models. In particular, the most active Cu(II) complex significantly inhibited cell proliferation with an IC₅₀ value lower than 1 μM; this effect was associated with a block of the cell cycle in the G₂/M phase. This Cu(II) complex induced neither the production of reactive oxygen species (ROS) nor the accumulation of p53 protein, suggesting the lack of DNA damage.

KEYWORDS: thiosemicarbazone; copper(II) complex; 8-hydroxyquinoline; proliferation; albumin; anticancer

ABBREVIATIONS: amino-terminal copper and nickel binding (ATCUN), circular dichroism (CD), dimethylformamide (DMF), dimethyl sulfoxide (DMSO), diethylenetriamine (Dien), ethylenediaminetetraacetic acid (EDTA), human serum albumin (HSA), 4-(2-hydroxyethyl)-1-piperazine ethanesulfonic acid (HEPES), root mean square deviation (RMSD), reactive oxygen species (ROS), non-small-cell lung carcinoma (NSCLC)

1. Introduction

Thiosemicarbazones are a well-known class of ligands, with a broad spectrum of biological activities, but newly, recovering the brilliant title of a recent paper, [1] they “turn from the old to new”. α -N-heterocyclic thiosemicarbazones, in fact, seem to be promising candidates for cancer therapy, in particular 3-aminopyridine-2-carboxaldehyde thiosemicarbazone (Triapine, **Scheme 1A**), which has been already investigated in numerous clinical phase trials, and some di-2-pyridylketone thiosemicarbazones (**Scheme 1B**; di-2-pyridylketone-4-cyclohexyl-4-methyl-3-thiosemicarbazone is entering clinical phase I studies) [2]. Notably, some thiosemicarbazones are reported to overcome P-gp-mediated drug resistance [3,4]. The reason of the anti-neoplastic activity of thiosemicarbazones is not completely understood, but it is in general connected with their possibility to chelate intracellular iron and to interact with the activity of the enzyme ribonucleotide reductase, which is very sensitive to the iron concentration. The chelation properties of thiosemicarbazones can be exploited also to target copper(II) and copper(II) homeostasis [5,6]. Iron and copper are involved in the Haber-Weiss reaction and in the production of oxygen reactive species, so iron and copper complexes of thiosemicarbazones are supposed to act by induction of oxidative stress [5,7], but other pathways have probably to be considered [8,9]. Triapine and di-2-pyridylketone thiosemicarbazones are fundamentally NN'S tridentate ligands, but also N₂S₂ tetradentate chelating bis(thiosemicarbazone) ligands and their Cu(II) complexes (**Scheme 1C**) have shown promising anticancer activity [10,11,12]. Moreover, the copper(II) complex of diacetyl bis(thiosemicarbazone) has shown hypoxia selectivity and it seems interesting as radiopharmaceutical for the imaging of hypoxic tissues [13]. Redox processes are involved also in the antineoplastic action of bis-thiosemicarbazones. The activity of the free ligands is attributed to their chelation properties towards essential ions as copper, so that the active species is the neutral copper(II) bis(thiosemicarbazone) complex. It enters the cell and, once inside, Cu(II) is reduced to Cu(I); finally, reduction is accompanied by dissociation of the metal ion and general poisoning of the cell [12].

In medicinal chemistry, 8-hydroxyquinoline is a very interesting pharmacophoric group: it is a “privileged structure” [14], whose biological properties are generally related to its chelating abilities [15]. Some 8-hydroxyquinoline derivatives [16] and also some of their metal complexes [17] have shown *in vitro* cytotoxicity against human cancer cell lines.

In light of these considerations and of some previous results [18], we decided to study the chelating properties of 8-hydroxyquinoline thiosemicarbazones **1-3** (**Scheme 2**), in particular towards copper(II) and, for comparison, also towards the non-redox-active zinc(II) ion. These ligands are diprotic, as the bis-thiosemicarbazones, but ONN'S tetradentate. The corresponding complexes **4-9** (**Scheme 2**) were characterized in solution and in the solid state, and, for the copper(II) complexes, also by means of quantum mechanical calculations and X-ray diffraction. Finally, *in vitro* antineoplastic properties are reported, together with some preliminary investigations on the mechanism of action of the copper(II) complexes.

2. Experimental

2.1 Materials and methods. Chemistry. All reagents of commercial quality were purchased from Sigma-Aldrich and used without further purification. The purity of the compounds was determined by elemental analysis and verified to be $\geq 95\%$ for all synthesized molecules. NMR spectra were recorded at 25 °C on a Bruker Avance 400 FT spectrophotometer. The ATR-IR spectra were recorded by means of a Nicolet-Nexus (Thermo Fisher) spectrophotometer by using a diamond crystal plate in the range of 4000-400 cm^{-1} . Elemental analyses were performed by using a FlashEA 1112 series CHNS/O analyzer (Thermo Fisher) with gas-chromatographic separation. Electrospray mass spectral analyses (ESI-MS) were performed with an electrospray ionization (ESI) time-of-flight Micromass 4LCZ spectrometer. MS spectra were acquired in positive EI mode by means of a DEP-probe (Direct Exposure Probe) mounting on the tip of a Re-filament with a DSQII Thermo Fisher apparatus,

equipped with a single quadrupole analyzer. UV–Vis spectra were recorded on an Evolution 260 Bio Thermo spectrophotometer by using cells of 1 cm path length.

2.2 Synthesis

2.2.1 Synthesis of 1-3. The thiosemicarbazone ligands were synthesized by condensation reaction of the proper thiosemicarbazide with 8-hydroxyquinoline-2-carboxaldehyde [18,19]. Thiosemicarbazide (1 mmol) was dissolved in warm ethanol (15 mL) and added of a solution of 8-hydroxyquinoline-2-carboxaldehyde (1 mmol, 0.173 g) in ethanol (15 mL). The resulting mixture was heated under reflux for 4 h; the precipitate was subsequently filtered, washed with cold ethanol and dried under vacuum.

8-Hydroxyquinoline-2-carboxaldehyde thiosemicarbazone (1). Yellow powder. Yield = 89%. ¹H-NMR (DMSO-d₆, 25°C), δ: 11.84 (s, 1H, NH), 9.84 (s, 1H, HO), 8.42-8.44 (2H, HC=N+ArH); 8.31-8.27 (d+s, 3H, ArH+NH₂); 7.37-7.44 (m, 2H, ArH); 7.10 (d, 1H, ArH, J = 7.1 Hz). ¹H-NMR (MeOD-d₄, 25°C), δ: 8.24 (3H, HC=N+ArH); 7.47 (t, 1H, ArH, J = 8.0 Hz); 7.39 (d, 1H, ArH, J = 8.4 Hz) 7.13 (d, 1H, ArH, J = 8.2 Hz). MS (EI, 70 eV, positive ions) m/z (%) = 245.9 ([M]⁺, 100). IR (cm⁻¹): ν_{OH}+ν_{NH2} = 3383, 3230; ν_{NH} = 3145; ν_{(C=C)+δ(N-H)+ν_{C=N} = 1605; ν_{C=S} = 1083, 840.}

8-Hydroxyquinoline-2-carboxaldehyde-4-ethyl-3-thiosemicarbazone (2). Yellow powder. Yield = 69%. ¹H-NMR (DMSO-d₆, 25°C), δ: 11.85 (s, 1H, NH), δ 9.84 (s, 1H, HO), 8.84 (s, 1H,NH), 8.42 (d, 1H, ArH, J = 8.4 Hz), 8.31 (d, 1H, ArH, J = 8.3 Hz), 8.26 (s, 1H, HC=N), 7.38-7.46 (m, 2H, ArH), 7.11 (d, 1H, ArH, J = 7.1 Hz), 3.64 (q, 1H, CH₂, J = 7.3 Hz), 1.19 (t,1H, CH₃, J = 7.4 Hz). MS(EI, 70 eV, positive ions) m/z (%) = 274.1 ([M]⁺, 100). IR (cm⁻¹): ν_{OH}+ν_{NH2} = 3400, 3298; ν_{NH} = 3142; ν_{C=N} = 1544; ν_{C=S} = 1098, 838.

8-Hydroxyquinoline-2-carboxaldehyde-4-phenyl-3-thiosemicarbazone (3). Yellow powder. Yield = 81%. ¹H-NMR (DMSO-d₆, 25°C), δ: 12.24 (s, 1H, OH), 10.37 (s, 1H, HN), 9.88 (s,1H, NH), 8.61 (d, 1H, ArH, J = 8.6 Hz), 8.37 (s, 1H, HC=N), 8.30 (d, 1H, ArH, J = 8.3 Hz), 7.58-7.38 (m, 6H, ArH), 7.27 (t, 1H, ArH, J = 7.2 Hz), 7.13 (d, 1H, ArH, J = 7.1 Hz). ¹H-NMR (MeOD-d₄, 25°C), δ: 8.32-8.26

(m, 3H, ArH+ HC=N), 7.67 (d, 2H, ArH, J = 7.6 Hz), 7.47-7.39 (m, 4H, ArH), 7.26 (t, 1H, ArH, J = 7.4 Hz), 7.14 (d, 1H, ArH, J = 7.6 Hz). MS-ESI (positive ions) m/z (%) = 323 ([M+H]⁺, 100); 345 ([M+Na]⁺, 90) 361 ([M+K]⁺, 50). IR (cm⁻¹): $\nu_{\text{OH}+\text{v}_{\text{NH}_2}}$ = 3408, 3320; ν_{NH} = 3138; $\nu_{\text{C=N}}$ = 1534; $\nu_{\text{C=S}}$ = 1091, 836.

2.2.2 Synthesis of the complexes 4-9. 0.1 g (0.4 mmol) of ligand were dissolved in degassed methanol under nitrogen and the pH was adjusted to 8-9 by adding NaOH 1M, resulting in an orange solution. An equimolar amount of Cu(CH₃COO)₂ · 2H₂O dissolved in methanol was added. Immediately, a dark precipitate formed, and the suspension was stirred for 2 hours at r.t.. The dark red powder was filtered off and washed with methanol.

The synthesis of Zn(II) complexes **7-9** proceeded in the same way, but by using Zn(CH₃COO)₂ · 2H₂O and ethanol as solvent.

(4). Dark red powder. Yield: 67%. MS-ESI (positive ions) m/z (%) = 308 ([CuL+H]⁺, 100). IR (cm⁻¹): ν_{NH_2} = 3246; $\nu_{\text{(C=C)}+\delta_{\text{(N-H)}}+\nu_{\text{C=N}}}$ = 1620; ν_{CS} = 1155, 838. Anal. Calcd. for C₁₁H₈CuN₄OS·0.5H₂O: C 41.70; H 2.86; N 17.68. Found: C 41.47; H 2.80; N 17.40.

(5). Dark red powder. Yield: 89%. MS-ESI (positive ions) m/z (%) = 336 ([CuL+H]⁺, 100); 358 ([CuL+Na]⁺, 50); 673 ([Cu₂L₂+H]⁺, 20); 695 ([Cu₂L₂+Na]⁺, 40). IR (cm⁻¹): $\nu_{\text{C=N}}$ = 1571; ν_{CS} = 1148, 834. Anal. Calcd. for C₁₃H₁₂CuN₄OS·H₂O: C 44.12; H 3.99; N 15.83. Found: C 44.61; H 4.33; N 15.60. Crystals suitable for X-ray diffraction analysis were obtained by slow evaporation of a methanolic solution of the powder.

(6). Dark red powder. Yield: 76%. MS-ESI (positive ions) m/z (%) = 384 ([CuL+H]⁺, 100); 769 ([Cu₂L₂+H]⁺, 60); 1152 ([Cu₃L₃+H]⁺, 50). IR (cm⁻¹): $\nu_{\text{C=N}}$ = 1595; ν_{CS} = 1123, 827. Anal. Calcd. for C₁₇H₁₂N₄OSCu 0.5 H₂O: C 51.97, H 3.33, N 14.26. Found: C 52.03, H 3.11, N 14.29.

(7). Orange powder. Yield: 67%. MS-ESI (positive ions) m/z (%) = 269 ([H₂L+Na]⁺, 100); 309 ([ZnL+H]⁺, 80). ¹H-NMR (MeOD-d₄, 25°C), δ : 8.41 (d, 1H, ArH, J = 8.42 Hz), 8.13 (s, 1H, HC=N), 7.65 (d, 1H, ArH, J = 7.65 Hz), 7.39 (t, 1H, ArH, J = 7.40 Hz), 7.06 (d, 1H, ArH J = 7.06 Hz), 6.87 (d, 1H, ArH, J = 6.89 Hz). IR (cm⁻¹): ν_{NH_2} = 3435, 3366; $\nu_{\text{(C=C)}+\delta_{\text{(N-H)}}+\nu_{\text{C=N}}}$ = 1592; ν_{CS} = 1096, 837.

Anal. Calcd. for $C_{11}H_8N_4OSZn \cdot 0.5 C_2H_5OH$: C 43.32; H 3.33; N 16.84. Found: C 43.40; H 3.25; N 16.98.

(8). Orange powder. Yield: 92%. MS-ESI (positive ions) m/z (%) = 241 ($[H_2L-S]^+$, 100); 336 ($[ZnL+H]^+$, 70). IR (cm^{-1}): ν_{NH_2} = 3331; $\nu_{C=N}$ = 1594; ν_{CS} = 1099, 836. Anal. Calcd. for $C_{13}H_{12}N_4OSZn \cdot 0.5 C_2H_5OH$: C 46.61; H 4.19; N 15.53. Found: C 46.60; H 4.03; N 15.82.

(9). Orange powder. Yield: 72%. MS-ESI (positive ions) m/z (%) = 291 ($[H_2L-S]^+$, 100); 385 ($[ZnL+H]^+$, 50). 1H -NMR (MeOD- d_4 , 25°C), δ : 8.43 (d, 1H, ArH, J = 8.42 Hz), 8.31 (s, 1H, HC=N), 7.69-7.65 (m, 3H, ArH), 7.43 (t, 1H, ArH, J = 7.40 Hz), 7.33 (m, 2H, ArH), 7.09-7.07 (m, 2H, ArH), 6.89 (d, 1H, ArH, J = 7.42 Hz). IR (cm^{-1}): ν_{NH_2} = 3321; $\nu_{C=N}$ = 1594; ν_{CS} = 1097, 837. Anal. Calcd. for $C_{17}H_{12}N_4OSZn \cdot 0.5 H_2O$: C 51.72; H 3.32; N 14.19. Found: C 52.10; H 3.49; N 13.85.

2.3 Studies in solution

Diethylenetriamine (Dien) trihydrochloride was prepared by dissolving high purity Dien in a small amount of ethanol; addition of few drops of concentrated HCl resulted in the appearance of a white microcrystalline precipitate which was filtered off and dried (purity > 99 % by potentiometric analysis). A Thermo Orion 720A pH-meter connected with a Hamilton glass electrode was used for pH measurements and potentiometric data collection. A 0.1 M KCl solution in methanol:water 9:1 (v/v) was used to fill the reference compartment of the electrode. The HEPES 25 mM buffer methanol:water 9:1 (v/v) solution at pH 7.4 was prepared as follows: solid HEPES (0.59 g) was suspended in 100 mL of a methanol:water 9:1 (v/v) mixture. Few drops of concentrated (10 N) aqueous NaOH solution were added until pH 7.4 was reached and complete dissolution of the solid was observed. Calibration of the glass electrode using buffers in methanol:water 9:1 (v/v) solutions was performed immediately before its use [20]. Stock solutions of the ligands (C_L = 1-1.1 mM, L = **1-3**) were prepared in DMF and used within few days. Stock solutions of $CuCl_2$ and $ZnCl_2$ in water (C_{Cu} ca. 0.016 M, C_{Zn} ca. 0.018 M) were prepared by weight of the salts and their titre determined using standardized EDTA solutions [21] Titrant metal solutions were obtained by dilution of the stock solutions in methanol:water 9:1 (v/v), and prepared at ca. 4 mM concentration. Titrant solution of

Dien ($C_{\text{Dien}} \text{ ca. } 11 \text{ mM}$) was prepared by weight from solid trihydrochloride salt. The salt was dissolved in HEPES 25 mM buffer methanol:water 9:1 (v/v) solution, and the pH corrected to 7.4 by addition of small aliquots of concentrated (10 N) aqueous NaOH solution.

2.3.1 UV-visible spectrophotometric titrations. The UV-vis spectra were collected using a Thermo Evolution 260 Bio spectrophotometer provided with a Peltier thermostat, and quartz cuvettes with 1 cm path length. Speciation diagrams were calculated using the HySS 2009 software [22]. The spectrophotometric titrations of the ligands **1-3** with Zn^{2+} were carried out as follows. Solutions of the ligands ($C_{\text{L}}^0 = 4\text{-}41 \text{ }\mu\text{M}$) were prepared in the cuvette by diluting with HEPES 25 mM buffer methanol:water 9:1 (v/v) solution (pH 7.4) a proper amount of the ligands stock solutions in DMF. The obtained ligand solutions were titrated with Zn^{2+} titrant solutions up to Zn:L 1.71 – 2.29. The Cu^{2+}/L (L = **1-3**) systems could not be studied by direct titrations with the metal since the stability constants of the copper(II) complexes are too high (*vide infra*). Competition UV-vis titration experiments were instead carried out using Dien as competing ligand. Sample solutions containing Cu^{2+} and the ligands in 1:1 *ratio* were prepared in the cuvette, in HEPES 25 mM buffer methanol:water 9:1 (v/v) solution (pH 7.4). These solutions were titrated with the Dien titrant solution, up to Dien: Cu^{2+} 13:1. Due to the relative slow attainment of the equilibrium conditions, each spectrum was collected 7 min after titrant addition and mixing. The logarithms of the conditional stability constants were calculated from the spectral dataset using HyperQuad 2006 software [23]. For each system, data from different titrations were treated together. Speciation diagrams were calculated using the HySS 2009 software [22]. Continuous variation (Job's) experiments were carried out by preparing 11 solutions with constant $C_{\text{Cu/Zn}} + C_{\text{L}}$ (ca. 41 μM ; L = **1-3**), and variable $C_{\text{L}}/(C_{\text{L}}+C_{\text{Cu/Zn}})$ molar fractions in the 0 – 1 range. All samples were prepared in HEPES 25 mM buffer methanol:water 9:1 (v/v) solution at pH 7.4.

2.3.2 Study of stability under aerobic condition. The stability under aerobic conditions of the Cu^{2+} complexes with **1-3** was studied by preparing Cu^{2+} :ligand solutions (1:1 *ratio*) directly in the cuvette ($C_{\text{Cu}} \text{ ca. } 40 \text{ }\mu\text{M}$) by adding proper amounts of copper(II) and ligands stock solutions. HEPES 25 mM

buffer methanol:water 9:1 (v/v) solution at pH 7.4 was used as medium. The cuvettes were sealed with a rubber stopper. A needle was inserted in the rubber stopper to allow maintain aerobic conditions in the cuvette and limiting the evaporation of the solvent. The solutions were left under stirring in the presence of atmospheric dioxygen, and the spectra registered every 30 min. for 10 h. There is a negligible variation of the spectra within this time frame.

2.3.3 Potentiometry. The potentiometric titrations of Dien and of the Cu²⁺/Dien systems were carried out in methanol:water 9:1 (v/v) mixtures at $T = 298.2 \pm 0.1$ K and $I = 0.1$ mol L⁻¹ (KCl) under a N₂ stream, using 50 mL samples. The potentiometric apparatus for the automatic data acquisition was already described [24,25]. The KOH solution used for potentiometric titrations was prepared by diluting a 10N KOH aqueous solution (Merck) to obtain a ca. 0.1 N KOH solution in methanol:water 9:1 (v/v). The titrant KOH solution was standardized in methanol:water 9:1 (v/v) against potassium hydrogen phthalate. The Cu²⁺ solution was prepared as reported above (stock solutions of CuCl₂). Both methanol and water used to prepare the samples for potentiometric titrations were boiled, cooled and stored under N₂ atmosphere, and used within few days. The electrode was calibrated in terms of [H⁺] by titrating HCl solutions with a standard KOH solution [26]. The Dien titrant samples were prepared by dissolving a weighted amount of the solid Dien trihydrochloride salt in methanol:water 9:1 (v/v). Three samples ($6.0\text{--}6.6 \cdot 10^{-3}$ mol L⁻¹) were titrated with KOH in the pH range 3.6-11.1. The Cu²⁺/Dien samples were prepared using a weighted amount of solid Dien trihydrochloride salt, to which aqueous Cu²⁺ was added, followed by proper amounts of methanol and water to afford the final titrant samples in methanol:water 9:1 (v/v). Three titrations were carried out with Dien:Cu²⁺ molar ratios from 2.5 to 3.1 ($C_{Cu} = 2.2\text{--}2.6 \cdot 10^{-3}$ mol L⁻¹) in pH range 3.1-11.2. The protonation and Cu²⁺ complexation constants were calculated from the potentiometric data using the HyperQuad 2009 program.²³ Least-squares treatment was performed by minimization of the sample standard deviation $\sigma = [\sum_i w_i (E_i^o - E_i^c)^2 / (n - m)]^{1/2}$, where E_i^o and E_i^c are the observed and calculated e.m.f. values, respectively, n is the number of observations and m is the number of refined parameters. The statistical weights w_i were put equal to $1/\sigma_i^2$, where σ_i is the expected error on each observed e.m.f. value (0.2

mV). A pK_w value of 14.41, determined from glass electrode calibration, was employed. For each system, data from different titrations were treated together. The conditional formation constants of the $[\text{Cu}(\text{Dien})]^{2+}$ and $[\text{Cu}(\text{Dien})_2]^{2+}$ complexes at $\text{pH} = 7.4$ were calculated by the HySS 2009 program,²² taking into account the formation of hydrolytic species of Cu^{2+} [27,28].

2.3.4 Interaction of the complex 4 with albumin. The study of the interaction of the Cu(II) complex **4** with albumin has been carried out in aqueous buffer HEPES solution 25 mM pH 7.4. A stock solution of commercial WT human serum albumin (HSA, Sigma) was prepared by weight at 300 μM concentration in the buffer solution. Due to the limited solubility in water, the stock solution of **4** (25 mM) was prepared by weight in DMSO. A 25 mM solution of $\text{CuCl}_2 \cdot 2 \text{H}_2\text{O}$ was also prepared by weight in DMSO. The samples for CD data collection in the visible range were prepared as follows: 2 ml of the HSA stock solution were added with either 10 μl of **4** or 10 μl of CuCl_2 solutions (control). The reference HSA spectrum was collected on a sample obtained by adding 10 μl DMSO to 2 ml of the HSA stock solution. The HSA:Cu ratio was 2.4. The samples for CD data collection in the UV range were prepared as follows: 250 μl of the HSA stock solution were added with either 2.5 μl of **4** or 2.5 μl of CuCl_2 solutions (control). The reference HSA spectrum was collected on a sample obtained by adding 2.5 μl DMSO to 250 μl of the HSA stock solution. The HSA:Cu ratio was 1.2. The blank spectrum was collected on a 250 μl HEPES buffer solution, added with 2.5 μl of DMSO. The spectra were collected on a Jasco J-715 UV-visible spectropolarimeter provided with a Peltier thermostat. Matched quartz cells of 10 or 1 mm path length were used for collecting spectra in the visible or UV range, respectively. The temperature was set to 25.0 $^\circ\text{C}$.

2.4 Crystallography.

A single crystal of **5** was mounted on a glass fibre and the intensity data were collected with a SMART APEX2 diffractometer with Bruker AXS CCD detector using Mo-K α radiation and a graphite crystal monochromator [$\lambda(\text{Mo-K}\alpha) = 0.71073 \text{ \AA}$]. The SAINT [29] software was used for integrating reflection intensities and scaling, and SADABS [30] for absorption correction. The structure was solved by direct methods using SIR97 [31] and refined by full-matrix least-squares on all F² using

SHELXL97 [32] implemented in the WinGX package [33]. All the non-hydrogen atoms in the molecules were refined anisotropically. The hydrogen atoms were partly found and partly placed in the ideal positions using riding models. The structure was solved by direct methods and difference Fourier synthesis using the SHELX suite of programs as implemented within the WINGX software. Thermal ellipsoid plots were generated using the program ORTEP-333 integrated within the WinGX suite of programs.

The crystal of **5** is monoclinic, space group $P2_1/c$; cell parameters: $a = 6.9669(6)$, $b = 13.063(1)$, $c = 15.831(1)$ Å, $\beta = 102.595(1)^\circ$, $V = 1406.1(4)$ Å³. The asymmetric unit is formed by a single molecule of formula C₁₃H₁₂CuN₄OS, Mr = 335.87, Z = 4, Dc = 1.59 g cm⁻³, $\mu = 1.756$ mm⁻¹, F(000) = 684. A semi-empirical absorption correction, based on multiple scanned equivalent reflections, has been carried out and gave $0.5934 < T < 0.7454$. A total of 17393 reflections were collected up to a θ range of 26.5° (± 8 h, ± 16 k, ± 19 l), 2914 unique reflections (Rint = 0.049). All non-hydrogen atoms were refined anisotropically. The hydrogen atoms were placed in ideal positions and refined using riding models.

CCDC1483582 contains the supplementary crystallographic data of **5** (http://www.ccdc.cam.ac.uk/data_request/cif; see also ESI).

2.5 Calculations.

Molecular orbital calculations were carried out using the D01 development version of Gaussian09 series of programs [34]. Two sets of geometries have been employed for electronic structure calculations: 1) pure square planar CuL complexes (SET-1); 2) Jahn-Teller distorted octahedral CuL complexes with two coordinating water molecules (SET-2). Several different DFT levels and basis sets have been employed: the hybrid functional B3LYP density functional [35,36,37] using the 6-31++G** (H. C. N. O. S) plus ECP-Lanl2DZ (Cu) (BS-I) and the hybrid functional of Truhlar and Zhao M06 density functional method [38] using the 6-31++G** (H. N. C. O. S) [39,40,41,42,43 44,45,46,47,48] and Los Alamos ECP plus TZ - Lanl2TZ(f) (Cu) [49,50,51] basis set (BS-II). Geometry SET-1 has been investigated both at BS-I and BS-II level, whereas SET-2 has been treated

at the level BS-II only. Optimized geometries and energies in the gas phase were computed with tight convergence criteria and the “nosymm” options were used for all optimizations. Cartesian coordinates in mol2 format for the optimized geometries and electronic energies for all compounds are provided in the Supporting Information. Vibrational frequencies were computed in the gas phase at the same level of theory and were used without scaling since the MO6 frequencies agree quite well with experimental values for a wide range of second and third period compounds [52]. Thermal corrections and free energies were calculated by standard statistical thermodynamic methods⁵³ using the unscaled DFT frequencies and the ideal gas/rigid rotor/harmonic oscillator approximations. Population analysis has been calculated within the Natural Bond Order approximation [54,55,56,57].

2.6 *Biology.*

2.6.1 *Cell culture.* Human non-small cell lung cancer (NSCLC) cell line A549, human breast cancer cell line MCF-7 and human MSTO mesothelioma cell line were obtained from American Type Culture Collection (ATCC) (Manassas, VA, USA) and cultured as recommended at 37°C in a humidified atmosphere of 5% CO₂ and 95% air. Stock solutions of 10 mM compounds were prepared in DMSO and diluted in fresh medium for use. The final concentration of DMSO never exceeded 0.1% v/v.

2.6.2 *Analysis of cell proliferation and cell cycle.* Cells were seeded into 96-well plate and exposed to various treatments. After 72 hours, cell proliferation was evaluated by crystal violet staining as previously described [58]. Briefly, crystal violet was solubilized in PBS with 0.2% TritonX-100 and the absorbance was measured at 570 nm. Data are expressed as percent inhibition of cell proliferation versus untreated cells. Distribution of cell population in the cell cycle was determined by propidium iodide staining and flow cytometry analysis [59].

2.6.3 *Western blot analysis.* Procedures for protein extraction, solubilisation and analysis by 1-D PAGE are described elsewhere [60]. Briefly 30-50 µg of proteins from cell lysates were resolved by 7.5% SDS-PAGE and transferred to PVDF membranes. Membranes were incubated with anti-phospho-mTOR (Ser2448); anti-mTOR; anti-phospho-P70S6K (Thr421/Ser424); anti-P70S6K; anti-

phospho-AKT (Ser473); anti-AKT; anti Cyclin B1 (Cell Signaling Technology, Beverly, MA, USA); anti-HSP72 (Stressgene Bioreagents, BE); anti-p53 (Santa Cruz Biotechnology, USA); anti-Actin (Sigma–Aldrich, St Louis, MO, USA). Blots were then washed and incubated with secondary HRP-coniugated antibodies (Pierce, Rockford, IL, USA). Immunoreactive bands were visualized using an enhanced chemiluminescence system (Immobilion™ Western Cemiluminescent HRP Substrate, Millipore, USA). The chemiluminescent signal was acquired by C-DiGit® Blot Scanner and the spots were quantified by Image Studio™ Software, LI-COR Biotechnology (Lincoln, NE).

2.6.4 Reactive oxygen species measurements. Intracellular hydrogen peroxide H₂O₂ and superoxide anion O₂⁻ were assessed by oxidation of the cell permeable fluorescent probes 5-(and-6)-chloromethyl-20,70-dichlorodihydrofluorescein diacetate, acetyl ester (CM-H2DCFDA, Molecular Probes®), and dihydroethidium (DHE, Merck Millipore), respectively as previously described [61]. Briefly, 3 x 10⁵ cells were incubated in absence or presence of the compound. During the last 30 min of treatment, the cells, loaded with CM-H2DCFDA 5 μM or DHE 5 μM, were left in the dark at 37 °C, and then trypsinized and analysed on a Beckman-Coulter EPICS XL flow cytometer.

2.6.5 Statistical analysis. Statistical analysis was carried out using GraphPad Prism 5.00 software. Statistical significance of differences among data was estimated by two-tailed Student's t test and P values are indicated where appropriate in the figures.

3. Results and Discussion

3.1 Synthesis. The thiosemicarbazone ligands **1-3** (**Scheme 2**) were synthesized in high yields by condensation of thiosemicarbazide or a 4-N-substituted-3-thiosemicarbazide with 8-hydroxyquinoline-2-carboxaldehyde. They were satisfactorily characterized by ¹H-NMR, IR, mass spectrometry and microanalysis. The ligands are in the *E* form in solution, as evidenced by the chemical shift values of the HC=N and NH proton in the ¹H-NMR spectrum in DMSO-d₆ [19,62]. **1-3**, in principle, can exhibit thione–thiol tautomerism: the absence of the S–H stretching band near

2600 cm^{-1} and the presence of a N–H stretching band at approximately 3150 cm^{-1} indicate that the thione form is the stable one; this is also confirmed by the $\nu(\text{C}=\text{S})$, coupled with $\text{N}=\text{C}=\text{N}$ stretching vibrations, observed at about 1100 cm^{-1} as a strong absorption [63].

The copper(II) and zinc(II) metal complexes **4-9** (**Scheme 2**) were obtained by reacting the acetate salts with the ligands **1-3** in ethanol or methanol, adjusting the pH at 8-9 with NaOH. In the IR spectra of **4-9** the absorptions of the NH and OH groups (around 3100 cm^{-1} and 3400 cm^{-1} in the ligand, respectively) disappeared, evidently because the ligand deprotonated upon complexation. In the spectra of the ligands the bands around 1530-1600 cm^{-1} were assigned to the iminic bond stretching vibrations; they underwent shifts of 15-60 cm^{-1} upon coordination, indicating the involvement of this group in coordination. In the ^1H NMR of the zinc(II) complexes **7** and **9** in DMSO- d_6 , a partial decoordination of the ligand and the presence of several chemical species were observed. On the other hand, in methanol- d_4 , there is a unique set of signals with a shift of the protonic resonances of about 0.2-0.3 ppm vs the free ligand. Elemental analysis and ESI-mass analysis indicated the presence of a complex with a 1:1 metal to ligand *ratio*. Overall, the data suggested the formation of a 1:1 metal chelate for all the complexes **4-9**, with the bis-deprotonated ligand behaving as an ONN'S donor system. In the case of **5**, the proposed structure was confirmed by X-ray diffraction analysis.

3.2 X-ray discussion. The molecular structure of copper(II) complex **5**, as determined by single-crystal X-ray crystallography, is reported in **Figure 1**.

The geometry of the Cu(II) coordination is square planar with the four donor atoms deriving from the dianionic tetradentate ligand, and namely the deprotonated phenolic oxygen, the nitrogen of the substituted quinoline ring, the iminic nitrogen and the thiolate sulfur. The coordination plane can be described as a 5-5-5 (*O,N,N,S*) chelate ring system. The copper atom lies exactly on the average plane formed by the four donor atoms, but its geometry is slightly distorted from the ideal square planar being the bite angles N2–Cu–S1 85.5(2)°, N2–Cu1–N1 78.27(2) and N1–Cu–O1 82.3(2)°. The Cu–S bond distance, 2.220(2) Å, and Cu–N(iminic) distance, 2.011(6) Å, are similar to those observed in analogous systems [19,64]. Upon coordination, the thiosemicarbazone moiety undergoes

deprotonation and gives an overall dianionic ligand. Thiosemicarbazones normally present a thione-thiol tautomerism and the deprotonation, concomitant to the coordination of the metal centre, brings to the stabilization of the thiolate form. This is apparent, in our case, from the length of the C11–S1 distance of 1.760(8) Å that suggests a thiol character, since it is much longer than the distances observed in free thiosemicarbazones (the average value of 431 non deprotonated structures found in the CSD [65,66] is C–S = 1.63(1) Å). The N3–C11 bond distance of 1.320(9) Å, accordingly, is markedly shorter than the average 1.35(1) Å of the free thiosemicarbazones of the same set, suggesting a double bond-like character.

The packing in the crystal is characterized by two main features: the hydrogen bond that connects the terminal amino nitrogen and the phenolic oxygen of an adjacent complex (**Figure SI1** and **SI2**), and the formation of stackings with π - π interactions of the aromatic systems. The first interaction leads to the formation of ribbons of molecules developing in the *b* direction of the unit cell, while the stackings extend in the *a* direction.

3.3 Quantomechanical calculation. We first wanted to investigate the electronic effects of the R groups of the ligands **2** and **3** (**Scheme 2**) on the structural properties of their complexes (Cu(II)EtL and Cu(II)PhL, respectively). We fully optimized the square planar structures (SET-1) generated by complexation between Cu²⁺ and the ligands, substituting the functional group R = NHC₂H₅ in **2** with R = NHCH₃ (Cu(II)MetL) for simplicity; we left methanol co-crystallization molecules as reported in one structure in the literature [19]. Despite the different electron withdrawal properties of the R groups, a substantially unmodified chelation ring was obtained (**Figure SI3**). Then, we considered the square planar structures optimized starting from a distorted octahedral geometry obtained placing two water molecules in the axial positions (SET-2). **Figure 2** shows the optimized structures of the aquo complexes Cu(II)MetL (a), Cu(II)EtL (b), and Cu(II)PhL (c).

As expected for a d⁹ transition metal (i.e. Cu²⁺) in all the three complexes the initial octahedral geometry relaxes to a square planar, with the originally coordinated water molecules now loosely interacting either with the metal or the alkoxy group. The square planar configuration is also

supported by the molecular orbital analysis that, in agreement with a doublet spin multiplicity, shows a remarkable spin polarization effect stabilizing the alpha electrons more than the beta ones. (**Figure SI4**). In agreement with a d^9 square planar coordination the hole in the Cu d orbitals is located in the high-energy $d_{x^2-y^2}(\text{Cu})+\sigma(\text{ligand})$ (**Figure SI4**) and the HOMO (**Figure SI5**) is localized on the atoms involved in the metallic coordination with an overall d_{xz} symmetry. Moreover, the HOMO does not involve the water molecules nearby the metallic center, that would bring the square planar coordination to a square pyramidal. Lastly, the LUMO is characterized by a marked $d_{x^2-y^2}$ orbital associated to the spin beta vacancy and a substantially ligand-dominant character for the spin alpha component.

The structural analysis of the complexes reported in **Figure 2** interestingly shows that both with the mild electron donors (i.e. $-\text{CH}_3$ and $-\text{CH}_2\text{CH}_3$) and the withdrawal (i.e. Ph) substituents, the thioamide nitrogen results substantially planar (i.e. sp^2 hybridized). This is supported by the coplanarity between C12-N4(H)-C11 resulting in 179.95 , 175.76 and 178.8° dihedral angles, respectively for $-\text{CH}_3$, $-\text{CH}_2\text{CH}_3$ and Ph. Furthermore, the average N4-C11 distance (1.35 \AA) is compatible with primary amides (1.325 \AA , bond order 1.2).⁶⁷ This partial double bond can generate *E-Z* isomers. Despite experimental observation that characterized the *E* isomer (complex **5**), DFT calculations showed that the *E* isomer is more stable than the *Z* one by only 0.5 kcal/mol , that is below the accuracy of the method. Still, an approximate estimation of the isomerization process revealed, as expected, significantly high energy ($\sim 10 \text{ kcal/mol}$) barrier justifying a possible kinetic control. In **Table 1** we compare the most relevant structural parameters obtained by the X ray diffraction analysis of **5**, with the relative calculated at the DFT-BS(I) and BS(II) level of accuracy. In the X-ray structure of **5** there are three five-membered chelation rings. The data calculated for this structure, with an *E* configuration around the amide bond, are reported in the DFT-BS(I) 5(E) and DFT-BS(II) 5(E) columns. Structures with 5,6,4-membered chelation rings are also known [19,68]; the structural details calculated assuming this isomer, with the thio- moiety involved in a 4 membered chelation to the metal, are reported in the DFT-BS(I) 4(E) column. Both computational levels (i.e. BS-(I) and BS-

(II)) predict with good accuracy the X-ray structure of **5**; in fact, extremely low RMSDs (root mean square deviation) on the atomic distances (D) and on the angular amplitudes (A) with respect the experimental data are obtained.

The DFT-BS(I) 4(E) structure obviously shows significant deviation from the experimental one, mostly ascribed to the Cu-S length which increases from ~ 2.35 Å to ~ 2.5 Å due to the more constrained four-membered ring. As a consequence, the iminic nitrogen compensates the partial positive charge created with a shorted Cu-N bond length (i.e. from ~ 2.08 Å to ~ 1.97 Å). Interestingly the two structures (with 5,5,5 membered or with 5,6,4 membered chelation rings) do not significantly differ in energy, leaving open the discussion for possible isomerization in solution or in the crystallization process [19].

3.4 Studies in solution. The conditional stability constants (hereafter indicated as β) of the Zn^{2+} complexes with the thiosemicarbazones **1-3** were determined in methanol:water 9:1 (v/v) (25 mM HEPES buffer, pH 7.4) by direct spectrophotometric UV-visible titrations of solutions of the ligands with a Zn^{2+} solution. A representative spectral set for the titration of **2** with Zn^{2+} is reported in **Figure 3** (for **1** and **3** with Zn^{2+} see **Figures SI6** and **SI7**). The spectrum of the ligands presents two bands at 308 and 343 nm, which decrease upon addition of Zn^{2+} . Two bands at 327 and 395 nm associated to the formation of complex species appeared upon addition of Zn^{2+} , and an isosbestic point is present at 371 nm.

The absorbance values at 395 nm for the titration of **2** as a function of the equivalents of Zn^{2+} added shows a titration end-point that is consistent with the addition of 1 eq. of Zn^{2+} *per* ligand, suggesting the presence of a $\text{Zn} + \text{L} = [\text{ZnL}]$ complexation equilibrium (charges omitted, $\text{L} = \mathbf{1} - \mathbf{3}$; **SI8-10**). Plots of the absorbance values at 395 nm from spectra of samples containing different Zn^{2+} /ligand molar fractions, and constant $C_{\text{Zn}} + C_{\text{L}}$ concentrations, clearly evidenced maxima at molar fraction of ligand = 0.5, confirming the formation of a Zn:L 1:1 species (Job's plots for **1-3**, **Figures SI11-SI13**). The treatment of the data of the spectroscopic titrations allowed to determine the conditional $\log \beta$ values for the $[\text{ZnL}]$ complexes, which are reported in **Table 2**.

We attempted the study of the complex formation equilibria for **1-3** with Cu^{2+} through direct spectrophotometric titrations of the ligands with the metal ion, in analogy with Zn^{2+} . The spectral dataset for the titration of **2** with Cu^{2+} and the plot of the absorbance values at 418 nm as a function of the equivalent of the metal are reported in **Figure 4**; the spectral changes are fully consistent with those reported for similar systems [18,19].

A sharp break of the formation curve is observed at 1 eq. of metal added, which indicates that the $\log\beta$ of the complex species are too high for being determined by these direct titration experiments. It is noteworthy, however, that the titration end-point, corresponding to 1 eq. of Cu^{2+} added, is consistent with the results of the Job's plots carried out for all **1-3** ligands (**Figures SI14-SI16**). Overall, these data suggest that the species formed are $\text{Cu}^{2+}:\text{L}$ 1:1, that is $[\text{CuL}]$.

We decided to determine the $\log\beta$ values of the copper(II) complexes by competition experiments based on the $[\text{CuL}] + \text{L}' = [\text{CuL}'] + \text{L}$ reaction, where L' is the competing polydentate ligand diethylenetriamine (Dien). These experiments were carried out by titration with Dien of solutions containing the $[\text{CuL}]$ complexes obtained by addition *in situ* of 1 eq. of Cu^{2+} to the ligands. A representative titration with Dien of a solution containing Cu^{2+} and **2** in 1:1 *ratio* is reported in **Figure 5** (the titrations with the other ligands are reported in the Supporting Information paragraph as **Figures SI17 and SI18**). Upon addition of Dien the absorbance of the bands at ca. 308 and 343 nm increases, while the two bands associated to the complex at ca. 418 and 490 nm decrease concomitantly. It is important to note that each spectrum was collected 7 minutes after the addition of Dien, as we observed that the spectrum changes within the first 3-4 min after titrant addition and mixing, while there are no spectral changes after 5 min. This behavior is attributed to a relative slow kinetics for the displacement of the thiosemicarbazone ligands by Dien.

The conditional $\log\beta$ values of the $\text{Cu}^{2+}/\text{Dien}$ complexes at pH 7.4 in methanol:water 9:1 (v/v) were in turn required to calculate the conditional $\log\beta$ value for the $[\text{CuL}]$ complex. We have therefore carried out a potentiometric study of the $\text{Cu}^{2+}/\text{Dien}$ system in methanol:water 9:1 (v/v) with the aim to determine the speciation of the system and to calculate the conditional $\log\beta$ values of the

complexes from their global formation constants. The protonation and complex formation constants of the Cu²⁺ complexes with Dien in this medium are reported in the Supporting Information (**Figures SI19** and **SI20**). The complex species found by potentiometry are [Cu(Dien)]²⁺, [Cu(HDien)(Dien)]³⁺ and [Cu(Dien)₂]²⁺. Known the speciation model, it was possible to calculate the concentration of all copper(II) and Dien species in solution at pH 7.4 using the Hyss 2009 software.²² Noteworthy, for total C_{Cu} ca. 40 μM at pH 7.4 the Cu:Dien 1:2 species ([Cu(HDien)(Dien)]³⁺ and [Cu(Dien)₂]²⁺) account to ca. 4 % total copper, therefore negligible. The conditional binding constant of Dien for Cu²⁺ was then calculated as:

$$\beta_{\text{Cond [CuDien]}} = \frac{[\text{CuDien}]}{[\text{Cu not bound to Dien}][\text{Dien not bound to Cu}]}$$

and it resulted to be 13.50 at pH 7.4.

By treating the spectral dataset as reported in **Figure 5** using the conditional binding constant of Dien for Cu²⁺, the calculated log β values for the Cu²⁺ + L = [CuL] equilibria are 14.56, 14.67 and 15.65 for L = **1**, **2** and **3**, respectively (**Table 2**). It is worth noting that the [Cu(Dien)]²⁺ complex has a significant absorption in the visible range only at ca. 600 nm (ε ca. 80 cm⁻¹ M⁻¹), its contribution to the absorbance is less than 0.01 at 600 nm, and thus negligible in the entire visible range [69]. For this reason, we calculated the conditional log β of formation of [CuL] by treating the absorbances in the 400-540 nm range.

3.5 Interaction of 4 with albumin. Albumin (HSA) is a plasma constituent present in concentrations close to mM [70]. It is known to bind copper(II) at the N-terminal ATCUN fragment with affinities of the order of pM (pH 7.4) [71]. Therefore, it is a potential competing ligand for Cu²⁺ in physiological media. In order to gain insight on the stability of the Cu(II) complex **4** in the presence of albumin, we collected the CD spectra in the visible range of solutions containing HSA at 300 μM concentration and in 1.2- to 2.4-fold excess with respect of **4**. As a fingerprint of Cu²⁺ complexation we used the Cotton effect which appears at ca. 500-600 nm in the visible CD spectra, that is known

to be diagnostic of the binding of Cu^{2+} to the ATCUN fragment [71]. The visible CD spectra of the solutions of HSA in presence of **4** or Cu^{2+} as chloride salt are reported in **Figure 6**.

The solution of free HSA does not present, as expected, any CD signal in the 400-800 nm range. Conversely, the solution of HSA and Cu^{2+} as chloride salt presents two CD bands at 490 nm (positive) and 570 nm (negative), which indicate the binding of copper(II) at the ATCUN site of the protein. Interestingly, the spectrum of the HSA/**4** solution does not present any Cotton effect associated to the binding of copper(II) to the ATCUN fragment, therefore indicating that the complex is stable in the presence of the protein. Also the CD spectra in the 300-500 nm range appear quite interesting (**Figure 7**).

In this range, the spectra do not allow to differentiate free HSA to that binding the copper(II) ion. However, it is clear that the HSA/**4** solution provides with spectral feature that are not accounted by simple Cu^{2+} ion-protein interaction. The Cotton effect of the HSA/**4** solution corresponds very well in wavelength and, remarkably, also in intensity, with the UV-visible absorption spectrum of **4** (**Figure 7**). It seems that not only **4** remains undissociated in the presence of HSA, but also it interacts with the protein to provide a signal in the CD spectrum. It is known that HSA has multiple binding sites and pockets into which a variety of drugs can be accommodated [72]. The CD data in our hands do not allow to put forward the structural nature of the HSA/complex adduct, which might involve the interaction of **4** into a pocket of HSA and/or the formation of hydrogen bonds on the protein surface. Nevertheless, **4** becomes CD active likely as the result of second sphere interactions: therefore, not only **4** is stable in the presence of the strong Cu(II) binding agent HSA, but the protein may also act as a carrier for the complex in plasma medium.

3.6 Effect on cell proliferation of A549 and MCF-7 cells. In order to evaluate the ability of the compounds to inhibit cell proliferation, we treated A549 NSCLC cells and MCF7 breast cancer cells with 10 μM of the ligands **1-3**, the copper(II) complexes **4-6** and the zinc(II) complex **9**. The zinc complex was chosen because zinc(II) ion is not redox active, on the contrary of copper(II) ion. As shown in **Figure 8** (A and B), **1** and **2** reduced cell proliferation up to 50% in A549 cells, whereas in

MCF7 cells they exhibited maximal inhibition of cell growth; also **3** and **9** showed a strong growth-inhibitory effect on MCF7 cells, but they were significantly less active with A549. Only the copper(II) complexes **4-6** completely inhibited cell proliferation in both cell lines. Compared to the analogous copper complex **6**, the zinc coordination compound **9** shows reduced activity: especially towards A549 cells, inhibition of cell proliferation is around 20%, compared to a complete inhibition induced by the analogous copper compounds. This indicates a crucial role of the metal ion features in determining activity. An investigation on the possible involvement of ROS production in the apoptosis process is presented in the following paragraph.

Based on these results, **4-6** were chosen for further studies. Firstly, A549 cells were treated with increasing doses of **4-6** for 3 days. As demonstrated in **Figure 9**, these compounds showed comparable dose-response curves, with IC_{50} of 0.5, 0.3 and 0.7 μM , respectively; comparable effects were obtained in MSTO mesothelioma cancer cells (data not shown). Note that the IC_{50} of the potent antineoplastic 2-benzoylpyridine 4-ethyl-3-thiosemicarbazone is practically equal, i.e. $IC_{50} = 0.593 \pm 0.148 \mu\text{M}$ [73] (for comparison, IC_{50} against A549 cells: cisplatin 11.92 ± 2.19 [74]; doxorubicin 1.8 ± 0.85) [75]. The slight differences in IC_{50} values (0.5, 0.3 and 0.7 μM , for **4**, **5** and **6** respectively) could be related to the different substituent at the hydrazonic moiety ($R = \text{H}$, ethyl, phenyl) resulting in different lipophilicity and thus in different ability to carry the metal ion throughout the cell membrane [77].

Then, we investigated the effects of **5** on A549 cell cycle distribution. As shown in **Figure 10**, **5** at 1 μM increased the percentage of cells in G_2/M phase compared to untreated cells (19.5 vs 9.6), suggesting that the observed inhibition of cell proliferation was mediated by a block in this phase of the cell cycle.

3.7 The copper(II) complex 5 did not induce cell stress. Treatment of A549 cells with **5** at 1 μM concentration induced an increase of Cyclin B expression, indicative of a block in G_2/M phase, but no accumulation of p53 protein was observed (**Figure 11**). Previous studies reported that the anti-proliferative activity of some copper(II) based-compounds is associated with the production of

reactive oxygen species⁷ and, in general, with the induction of intracellular stress. To evaluate whether our compounds produce the same effects, firstly we quantified the levels of HSP72, a well-known stress-induced protein [76], in A549 cells treated with **5** at 1 μ M concentration. As reported in **Figure 11**, the inducible level of HSP72 did not change. In addition, A549 cells were treated with 0.5 and 1 μ M of **5** and ROS formation was evaluated by flow cytometry using CM-H2DCFDA and DHE oxidant-sensitive fluorescent detection probes. We do not detect ROS production after treatment with **5** at concentrations comparable or higher than IC₅₀ (data not shown) for 24 and 48 hours. These observations are in accord with mechanistic studies on copper derivatives of Triapine and other thiosemicarbazones, underlying that thiol-induced intracellular ROS generation might contribute to the anticancer activity of copper thiosemicarbazone complexes, but is not the determining factor [8]. The antiproliferative activity of the Cu(II) complexes is therefore correlated to diverse mechanisms of action; in the literature alternative mechanisms are also proposed: for example, Cu(II) thioxotriazole complexes induce cell death via paraptosis [77]. Other copper(II) compounds activated a mechanism, that is based on the arrest of the cell in the S phase and induction of apoptosis by intrinsic pathway, with increased ROS accumulation [78]. An interesting evaluation of the Topo II α inhibition activity of a series α -heterocyclic-N4-substituted thiosemicarbazones and their corresponding copper complexes was also reported [79]. Therefore, further studies will be directed to explore the molecular mechanism of action of the synthesized copper compounds.

4. Conclusions

The hydroxyquinoline thiosemicarbazone ligands **1-3** form exclusively metal:ligand 1:1 species in solution with copper(II) and zinc(II), in agreement with the behavior of other previously reported similar thiosemicarbazones. The solid state structure of the copper(II) complexes is square planar, as results from quantum mechanical calculations and by the single crystal X-ray diffraction analysis of **5**. The Cu²⁺ complexes are more stable than the Zn²⁺ ones, as expected by the Irving-Williams series

and defined by solution studies. In this connection, note that the inhibition of cell proliferation produced by the Zn(II) complex **9** (**Figure 8**) can be due to partial transmetallation and formation in the cell of the more stable Cu(II) complex [80].

The Cu(II) complexes **4-6** are more active than the corresponding ligands towards NSCLC and breast cancer cell proliferation, with IC_{50} values ranging from 0.3 to 0.7 μ M in A549 cell line. On the contrary, the zinc(II) complex **9** showed reduced activity. The most active copper(II) complex **5** reduces cell proliferation with IC_{50} lower than 1 μ M, with an increase of cells in G2/M phase. Peculiarity of **5** is the absence of ROS-accumulation, in contrast with other copper(II) complexes which were shown to induce ROS-dependent cell stress and death.⁵ p53 accumulation is a sign of genotoxic stress accompanied by DNA damage [81]: the Cu(II) complex **5** did not cause increase of p53 levels in A549 cells wt for p53, indicating lack of DNA damage. Further studies are ongoing to explore the molecular mechanism of action of these compounds and to improve their selectivity.

Author Contributions

The manuscript was written through contributions of all authors. All authors have given approval to the final version of the manuscript.

Notes

The authors declare no competing financial interest.

ACKNOWLEDGMENTS

The authors thank “Centro Interfacoltà Misure Giuseppe Casnati” of the University of Parma for facilities. Thanks are also due to dr. Andrea Griesi for the collection of the UV data and the contribution to their elaboration. This investigation was supported by the association “Noi per Loro

Onlus”, project “Andrea Spadola”, Associazione Volontaria Promozione Ricerca Tumori (A.VO.PRO.RI.T.) (Parma), Cooperativa sociale “Di Mano in Mano Onlus” (Parma), and Associazione Augusto per la Vita (Novellara, Reggio Emilia).

Figure 1. ORTEP representation of the copper(II) complex **5** with ellipsoids at 50% probability

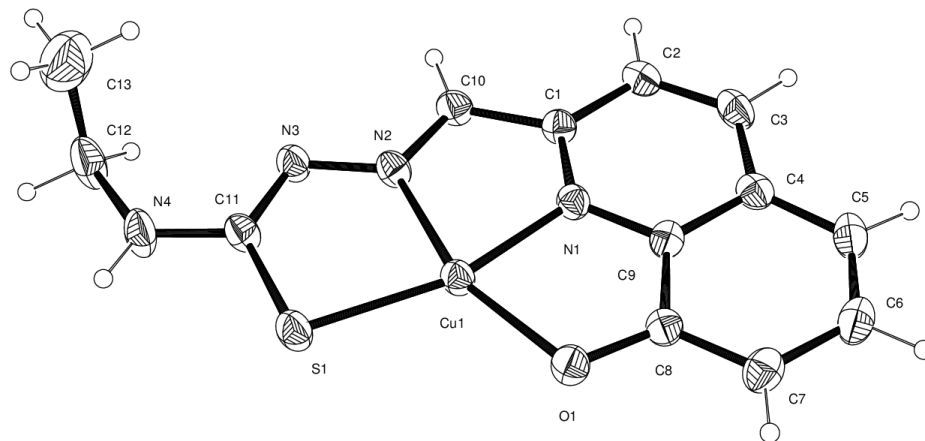


Figure 2. DFT-B3LYP structures optimized starting from the distorted octahedral geometry: a) Cu(II)MetL, b) Cu(II)EtL, and c) Cu(II)PhL aquo complexes.

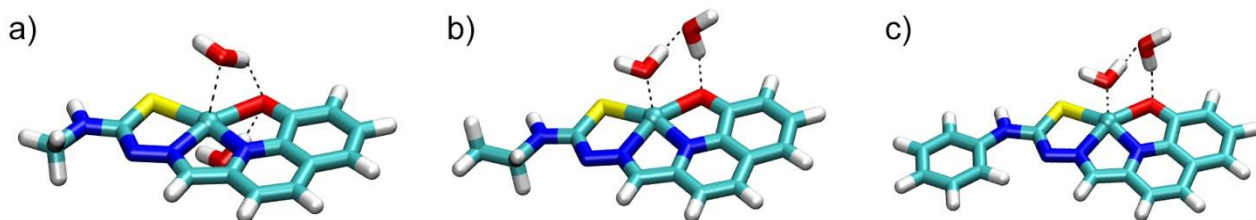


Figure 3. UV-visible spectrophotometric titration of L=2 with Zn²⁺ in methanol:water 9:1 (v/v) (25 mM HEPES buffer, pH 7.4, C_L⁰ = 41 μM, Zn:L = 0-1.81).

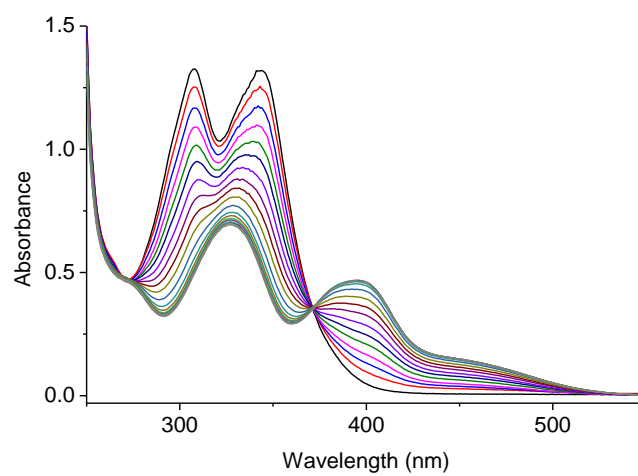


Figure 4. UV-visible spectrophotometric titration of **2** with Cu^{2+} in methanol:water 9:1 (v/v) (25 mM HEPES buffer, pH 7.4, $C_L^0 = 41 \mu\text{M}$, $\text{Cu:L} = 0\text{-}1.30$). Inset: absorbance values at 418 nm as a function of equivalents of Cu^{2+} added.

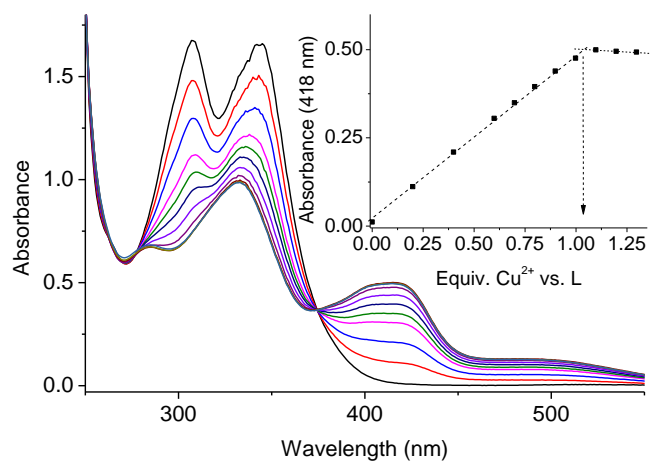


Figure 5. UV-visible spectrophotometric titration with Dien of a $\text{Cu}^{2+}/\mathbf{2}$ 1:1 solution in methanol:water 9:1 (v/v) (25 mM HEPES buffer, pH 7.4, $C_{\text{Cu}} = 38 \mu\text{M}$, Dien:Cu = 0-13); in black the spectrum of $\mathbf{2}$ ($41 \mu\text{M}$).

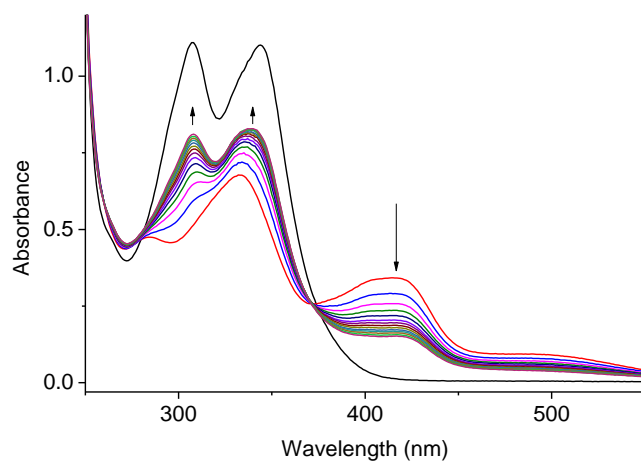


Figure 6. Visible CD spectra of solutions of HSA (300 μM , aqueous buffer HEPES solution 25 mM, pH 7.4). Black: free HSA; red: HSA with 0.42 eq. of $\text{CuCl}_2 \cdot 2 \text{H}_2\text{O}$; blue: HSA with 0.42 eq. of the Cu(II) complex **4**.

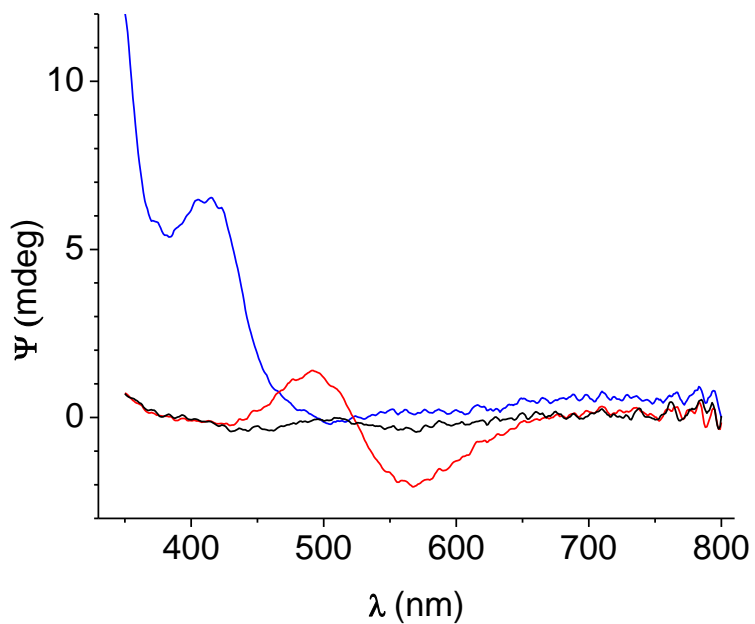


Figure 7. UV-visible CD spectra of solutions of HSA (300 μ M, aqueous buffer HEPES solution 25 mM, pH 7.4). Black: free HSA; red: HSA with 0.83 eq. of $\text{CuCl}_2 \cdot 2\text{H}_2\text{O}$; blue: HSA with 0.83 eq. of **4**. The green spectrum is that of a solution 41 μ M of **4** in methanol water 9:1 (v/v), HEPES buffer solution (25 mM, pH 7.4).

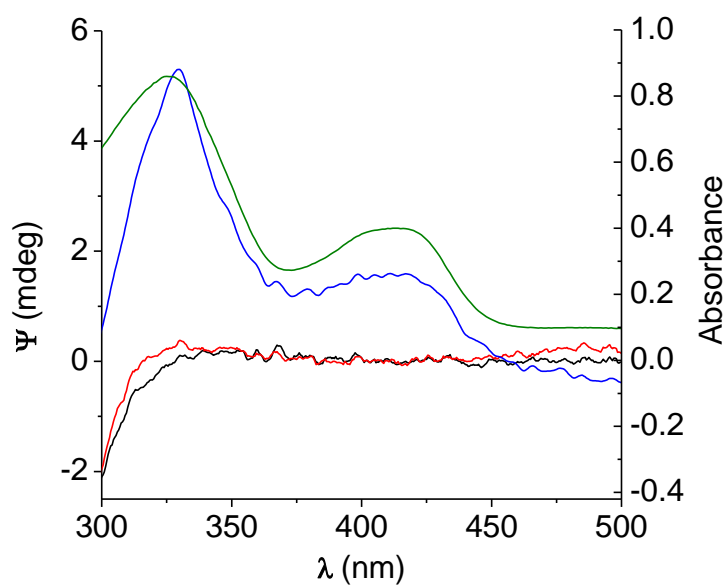


Figure 8. A549 (A) and MCF7 (B) cells were treated with the indicated compounds at 10 μ M for 3 days; then, cell proliferation was evaluated by crystal violet assay. Data are expressed as percent inhibition of cell proliferation \pm SD *versus* untreated cells. Experiments are the mean value of three independent measurements.

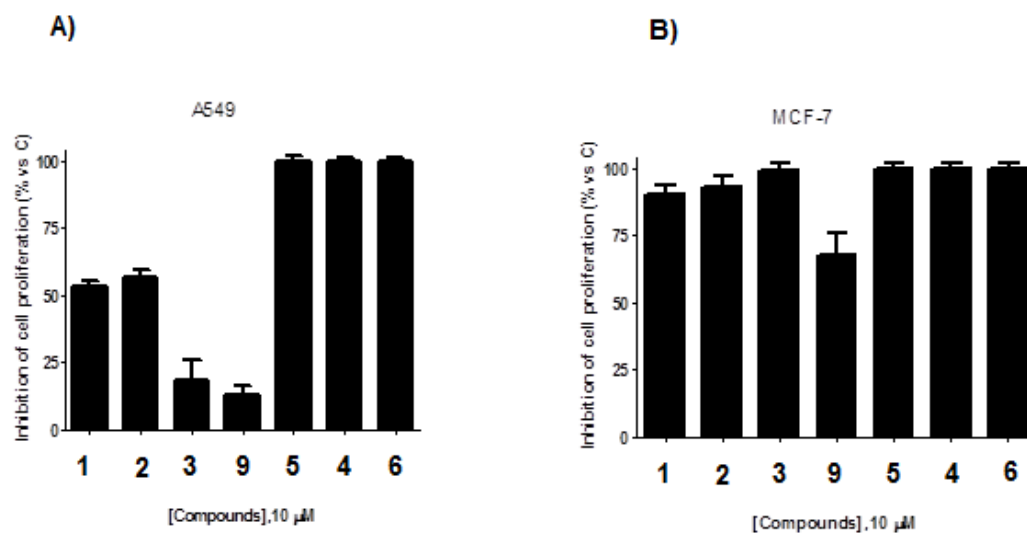


Figure 9. A549 cells were treated for 3 days with the copper(II) complexes **4**, **5** and **6**. Cell growth was evaluated by crystal violet assay and IC₅₀ were calculated by Graph Pad Prism 5.00 software. Experiments are the mean value of three independent measurements (\pm SD).

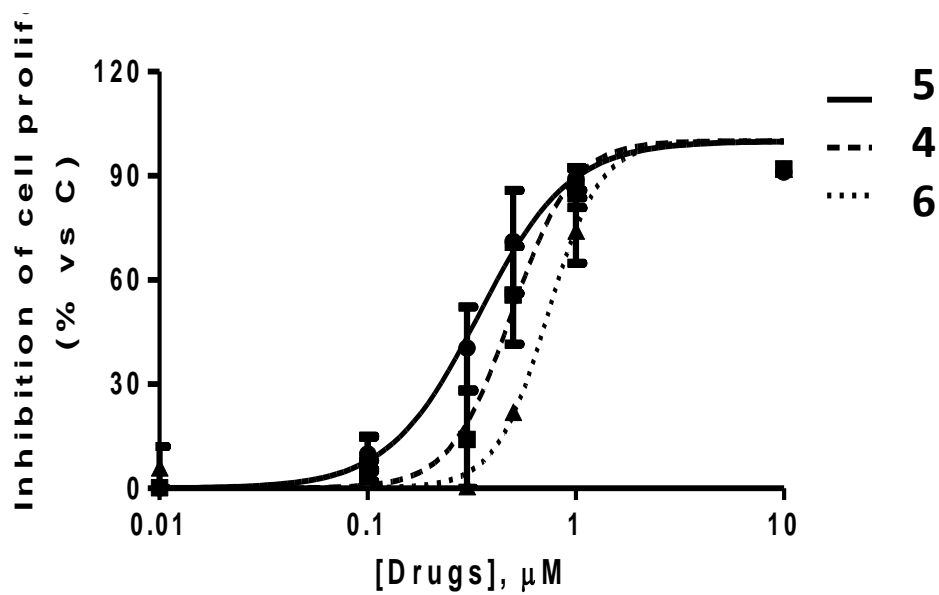
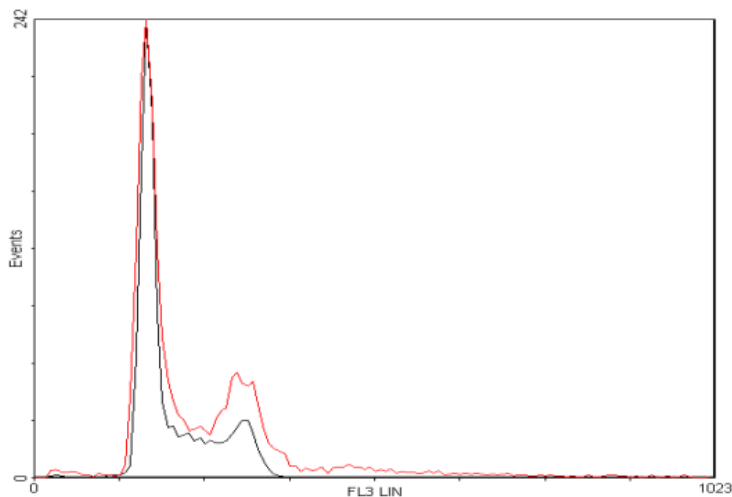
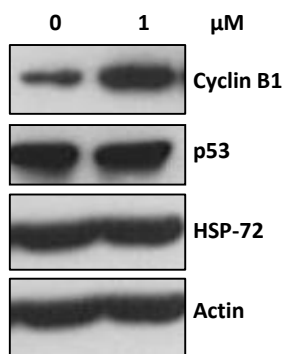


Figure 10. Cell cycle profile of A549 cells untreated (black line) and treated (red line) with compound **5** at 1 μM concentration for 48 h. Mean percentages \pm SD of cells residing in each cycle phase are reported. Experiments are the mean value of three independent measurements.

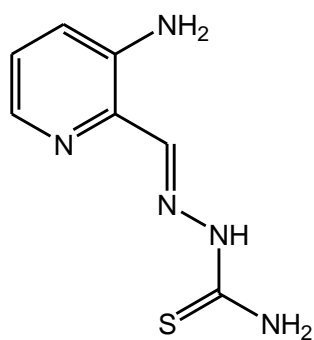


	Control	5 (1 μM)	P value
G ₀ /G ₁	58.8 \pm 1.4	55.0 \pm 2.3	0.034
S	31.6 \pm 2.4	25.5 \pm 5.9	0.11
G ₂ /M	9.6 \pm 2.7	19.5 \pm 7.2	0.04

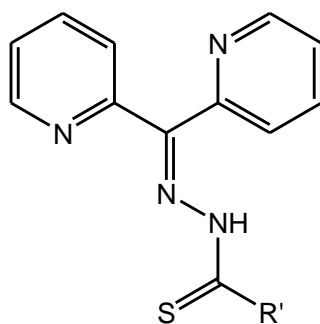
Figure 11. A549 cells were treated with **5** $1\mu\text{M}$ for 24h. Then western blot analysis was performed to evaluate Cyclin B, p53 and HSP72 protein levels.



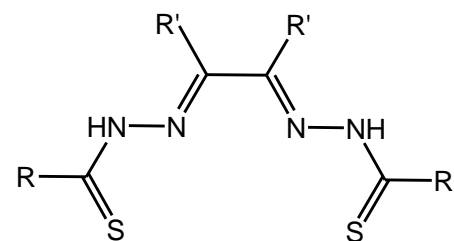
Scheme 1. Chemical structures of: (A) 3-aminopyridine-2-carboxaldehyde thiosemicarbazone (Triapine), (B) di-2-pyridylketone thiosemicarbazones and (C) bis(thiosemicarbazones).



(A)

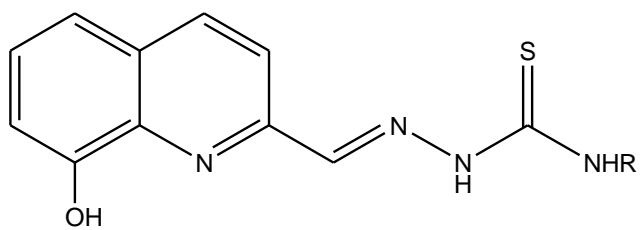


(B)

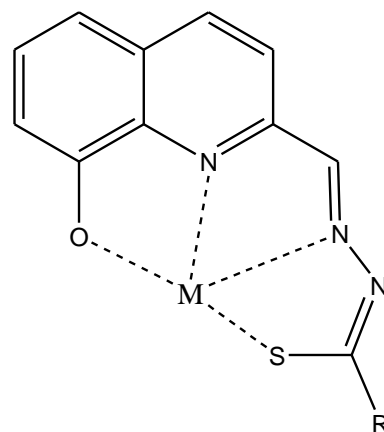


(C)

Scheme 2. Structures of the ligands (**1-3**) and of the metal complexes (**4-9**)



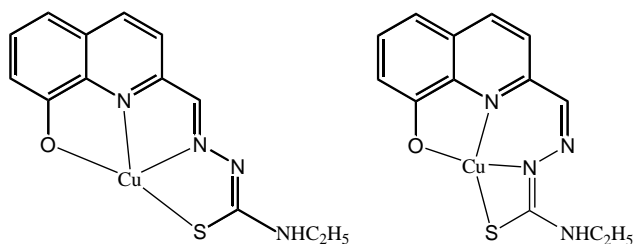
- R = H **(1)**
R = CH₂CH₃ **(2)**
R = Ph **(3)**



M = Cu(II)

M = Zn(II)

- | | |
|--|--|
| R = H (4) | R = H (7) |
| R = CH ₂ CH ₃ (5) | R = CH ₂ CH ₃ (8) |
| R = Ph (6) | R = Ph (9) |

Table 1

Param.	Exp E	DFT-BS(I) 5(E)	DFT-BS(II) 5(E)	DFT-BS(I) 4(E)
Cu-S	2.200	2.348	2.304	2.514
N2-Cu-S1	85.5	82.3	83.4	68.3
N2-Cu1-N1	78.3	78.0	78.0	88.7
N1-Cu-O1	82.3	79.8	81.6	83.5
Cu-N(iminic)	2.011	2.081	2.080	1.966
C11-S1	1.760	1.765	1.768	1.742
C11-N3	1.320	1.339	1.336	1.343
Relative Energy (kcal/mol)		0.0		0.0
RMSD-D (Å)		0.149	0.106	0.315
RMSD-A (°)		4.1	2.2	20.1

Table 2. Logarithms of the conditional formation constants of the Cu²⁺ and Zn²⁺ complexes of the ligands L=1-3 (methanol:water 9:1 v/v, 25 mM HEPES buffer, pH 7.4). The corresponding affinities of the ligands for the metal ions (K_a) are also reported. Standard deviations are in parentheses.

Ligand (L)	$\log \beta$	K_a
1		
[CuL]	14.56(1)	2.75(6) 10 ⁻³ pM
[ZnL]	6.68(1)	0.21(2) μM
2		
[CuL]	14.67(1)	2.14(5) 10 ⁻³ pM
[ZnL]	6.13(4)	0.74(7) μM
3		
[CuL]	15.65(1)	2.24(5) 10 ⁻⁴ pM
[ZnL]	7.30(1)	0.050(1) μM

References

- [1] Yu, Y.; Kalinowski, D.S.; Kovacevic, Z.; Siafakas, R.A.; Jansson, P.J.; Stefani, Ch.; Lovejoy, D.B.; Sharpe, P.S.; Bernhardt, P.V.; Richardson, D.R. Thiosemicarbazones from the Old to New: Iron Chelators That Are More Than Just Ribonucleotide Reductase Inhibitors. *J. Med. Chem.* **2009**, *52*, 5271–5294.
- [2] Britta, F.; Kryeziu, K; Kallus, S.; Heffeterb, P.; Bergerb, W.; Kowol, Ch. R.; Keppler, B. K. Nanoformulations of anticancer thiosemicarbazones to reduce methemoglobin formation and improve anticancer activity. *RSC Adv.* **2016**, *6*, 55848–55859.
- [3] Pati, M.L.; Niso, M.; Ferorelli, S.; Abate, C.; Berardi, F. Novel metal chelators thiosemicarbazones with activity at the σ_2 receptors and P-glycoprotein: an innovative strategy for resistant tumor treatment. *RSC Adv.* **2015**, *5*, 103131–103146.
- [4] Fung, K. L.; Tepede, A. K.; Pluchino, K. M.; Pouliot, L. M.; Pixley, J. N.; Hall, M. D.; Gottesman, M. M. Uptake of compounds that selectively kill multidrug-resistant cells: the copper transporter SLC31A1 (CTR1) increases cellular accumulation of the thiosemicarbazone NSC73306. *Mol. Pharmaceutics* **2014**, *11*, 2692–2702.
- [5] Santini, C.; Pelli, M.; Gandin, V.; Porchia, M.; Tisato F.; Marzano, C. Advances in copper complexes as anticancer agents. *Chem.Rev.* **2013**, *114*, 815-862.
- [6] Denoyer, D.; Masaldan, S.; La Fontaine, S.; Cater, M.A. Targeting copper in cancer therapy: 'Copper That Cancer'. *Metallomics* **2015**, *7*, 1459-1476.
- [7] Akladios, F.N.; Andrew, S. D.; Parkinson, Ch. J. Increased generation of intracellular reactive oxygen species initiates selective cytotoxicity against the MCF-7 cell line resultant from redox active combination therapy using copper–thiosemicarbazone complexes. *J Biol Inorg Chem* **2016**, *21*, 407–419.

-
- [8] Kowol, Ch. R.; Heffeter, P.; Miklos, W.; Gille, L.; Trondl, R.; Cappellacci, L.; Berger, W.; Keppler, B. K. Mechanisms underlying reductant-induced reactive oxygen species formation by anticancer copper(II) compounds. *J. Biol. Inorg. Chem.* **2012**, *17*, 409–423.
- [9] Wang, J.; Luo, C.; Shan, C.; You, Q.; Junyan Lu, J.; Elf, S.; Zhou, Y.; Wen, Y.; Vinkenburg, J.L.; Fan, J.; Kang, H.; Lin, R.; Han, D.; Xie, Y.; Karpus, J.; Chen, S.; Ouyang, S.; Luan, C.; Zhang, N.; Ding, H.; Merckx, M.; Liu, H.; Chen, J.; Jiang, H.; He, C. Inhibition of human copper trafficking by a small molecule significantly attenuates cancer cell proliferation. *Nature Chemistry* **2015**, *7*, 968–979.
- [10] Stefani, C.; Zaynab Al-Eisawi, Z.; Patric J. Jansson, P.J.; Kalinowski, D. S.; Richardson, D. R. Identification of differential anti-neoplastic activity of copper bis(thiosemicarbazones) that is mediated by intracellular reactive oxygen species generation and lysosomal membrane permeabilization. *J.Inorg.Biochem.* **2015**, *152*, 20–37.
- [11] Palanimuthu, D.; Shinde, S.V.; Somasundaram, K.; Samuelson, A.G. In Vitro and in Vivo Anticancer Activity of Copper Bis(thiosemicarbazone) Complexes. *J.Med.Chem.* **2013**, *56*, 722–734.
- [12] Paterson, B.M.; Donnelly, P. S. Copper complexes of bis(thiosemicarbazones): from chemotherapeutics to diagnostic and therapeutic radiopharmaceuticals. *Chem.Soc.Rev.* **2011**, *40*, 3005–3018.
- [13] Dearling, J. L. J.; Lewis, J. S.; Mullen, G. E. D.; Welch, M. J.; Blower, P. J. Copper bis(thiosemicarbazone) complexes as hypoxia imaging agents: structure–activity relationships. *J.Biol.Inorg.Chem.* **2002**, *7*, 249–259.
- [14] Song, Y.; Chen, W.; Kang, D.; Zhang, Q.; Zhan, P.; Liu, X. “Old friends in new guise”: exploiting privileged structures for scaffold re-evolution/refining. *Comb. Chem. High Throughput Screen.* **2014**, *17*, 536–553.
- [15] Song, Y.; Xu, H.; Chen, W.; Zhan, P.; Liu, X. 8-Hydroxyquinoline: a privileged structure with a broad-ranging pharmacological potential. *Med.Chem.Commun.* **2015**, *6*, 61-74.

-
- [16] Chan, H.S.; Chui, C.H.; Chan, S.W.; Kok, S.; Chan, D.; Tsoi, M.Y.T.; Leung, P.H.M.; Lam, A.K.Y.; Chan, A.S.C.; Lam, K.H.; Tang, J.C. Synthesis of 8-Hydroxyquinoline Derivatives as Novel Antitumor Agents. *ACS Med. Chem. Lett.* **2013**, *4*, 170–174.
- [17] Qin, Q.; Chen, Z.; Qin, J.; He, X.; Li, Y.; Liu, Y.; Huang, K.; Liang, H. Studies on antitumor mechanism of two planar platinum(II) complexes with 8-hydroxyquinoline: synthesis, characterization, cytotoxicity, cell cycle and apoptosis. *Eur. J. Med. Chem.* **2015**, *92*, 302-313, and references therein.
- [18] Zhang, H.; Thomas, R.; Oupicky, D.; Peng, F. Synthesis and characterization of new copper thiosemicarbazone complexes with an ONNS quadridentate system: cell growth inhibition, S-phase cell cycle arrest and proapoptotic activities on cisplatin-resistant neuroblastoma cells. *J. Biol. Inorg. Chem.* **2008**, *13*, 47-55.
- [19] Hickey, J.L.; Crouch, P.J.; Mey, S.; Caragounis, A.; White, J.M.; White, A.R.; Donnelly, P.S. Copper(II) complexes of hybrid hydroxyquinoline-thiosemicarbazone ligands: GSK3 β inhibition due to intracellular delivery of copper. *Dalton Trans.* **2011**, *40*, 1338-1347.
- [20] Tegoni, M.; Furlotti, M.; Tropiano, M.; Lim, C.S.; Pecoraro, V. L. Thermodynamics of core metal replacement and self-assembly of Ca²⁺ 15-metallacrown-5. *Inorg.Chem.* **2010**, *49*, 5190–201.
- [21] Vogel, A.I. *Quantitative Inorganic Analysis Including Elementary Instrumental Analysis*; Longmans: London, 1962.
- [22] Alderighi, L.; Gans, P.; Ienco, A.; Peters, D.; Sabatini, A.; Vacca, A. Hyperquad simulation and speciation (HySS): a utility program for the investigation of equilibria involving soluble and partially soluble species. *Coord.Chem.Rev.* **1999**, *184*, 311–318.
- [23] Gans, P.; Sabatini, A.; Vacca, A. Investigation of equilibria in solution. Determination of equilibrium constants with the HYPERQUAD suite of programs. *Talanta* **1996**, *43*, 1739–1753.
- [24] Dallavalle, F.; Tegoni, M. Speciation and structure of copper(II) complexes with (S)-phenylalanine- and (S)-tryptophanhydroxamic acids in methanol/water solution: a combined potentiometric, spectrophotometric, CD and ESI-MS study. *Polyhedron* **2001**, *20*, 2697–2704.

-
- [25] Fiscaro, E.; Braibanti, A. Potentiometric titrations in methanol/water medium: Intertitration variability. *Talanta* **1988**, *35*, 769-774.
- [26] Gran, G. Determination of the equivalence point in potentiometric titrations. Part II. *Analyst* **1952**, *77*, 661-671.
- [27] Pettit, L.D.; Powell, H.K. *The IUPAC Stability Constants Database*, Royal Society of Chemistry, London, 1992–2000.
- [28] Smith, R.M.; Martell, A.E.; Motekaitis, R.J. *NIST Critically Selected Stability Constants of Metal Complexes*, Database 46, 7.0, Gaithersburg, MD, USA, 2003.
- [29] SAINT: SAX, Area Detector Integration, Siemens Analytical Instruments Inc., Madison, Wisconsin, USA
- [30] Sheldrick, G. SADABS: Siemens Area Detector Absorption Correction Software, University of Goettingen, Germany, 1996.
- [31] Altomare, A.; Burla, C.; Camalli, M.; Cascarano, G.L.; Giacovazzo, C.; Guagliardi, A.; Moliterni, A.G.G.; Polidori, G.; Spagna, R. *J. Appl. Crystallogr.* **1999**, *32*, 115-119.
- [32] Sheldrick, G.M. *Acta Cryst.* **2008**, A64, 112-122.
- [33] Farrugia, L.J. *J. Appl. Crystallogr.* **1999**, *32*, 837-838.
- [34] M. J. Frisch, G. W. Trucks, H. B. Schlegel, G. E. Scuseria, M. A. Robb, J. R. Cheeseman, G. Scalmani, V. Barone, B. Mennucci, G. A. Petersson, H. Nakatsuji, M. Caricato, X. Li, H. P. Hratchian, A. F. Izmaylov, J. Bloino, G. Zheng, J. L. Sonnenberg, M. Hada, M. Ehara, K. Toyota, R. Fukuda, J. Hasegawa, M. Ishida, T. Nakajima, Y. Honda, O. Kitao, H. Nakai, T. Vreven, J. A. Montgomery Jr., J. E. Peralta, F. Ogliaro, M. Bearpark, J. J. Heyd, E. Brothers, K. N. Kudin, V. N. Staroverov, R. Kobayashi, J. Normand, K. Raghavachari, A. Rendell, J. C. Burant, S. S. Iyengar, J. Tomasi, M. Cossi, N. Rega, J. M. Millam, M. Klene, J. E. Knox, J. B. Cross, V. Bakken, C. Adamo, J. Jaramillo, R. Gomperts, R. E. Stratmann, O. Yazyev, A. J. Austin, R. Cammi, C. Pomelli, J. W. Ochterski, R. L. Martin, K. Morokuma, V. G. Zakrzewski, G. A. Voth, P. Salvador, J. J. Dannenberg,

S. Dapprich, A. D. Daniels, Ö. Farkas, J. B. Foresman, J. V. Ortiz, J. Cioslowski, D. J. Fox, Gaussian 09. Revision D.01. Gaussian, Inc., Wallingford CT. 2009.

[35] Lee, C.; Yang, W.; Parr, R. G. Development of the Colle-Salvetti correlation-energy formula into a functional of the electron density. *Phys. Rev. B.* **1988**, *37*, 785-89.

[36] Miehlich, B.; Savin, A.; Stoll, H.; Preuss, H. Results obtained with the correlation-energy density functionals of Becke and Lee, Yang and Parr. *Chem. Phys. Lett.* **1989**, *157*, 200-206.

[37] Becke, A. D. Density-functional thermochemistry. III. The role of exact exchange. *J. Chem. Phys.* **1993**, *98*, 5648-5652.

[38] Zhao, Y.; Truhlar, D. G. The M06 suite of density functionals for main group thermochemistry, thermochemical kinetics, noncovalent interactions, excited states, and transition elements: two new functionals and systematic testing of four M06-class functionals and 12 other functionals. *Theor. Chem. Acc.* **2008**, *120*, 215-241.

[39] Ditchfield, R.; Hehre, W. J.; Pople, J. A. Self-Consistent Molecular-Orbital Methods. IX. An Extended Gaussian-Type Basis for Molecular-Orbital Studies of Organic Molecules. *J. Chem. Phys.* **1971**, *54*, 724-728.

[40] Hehre, W. J.; Ditchfield, R.; Pople, J. A. Self-Consistent Molecular Orbital Methods. XII. Further Extensions of Gaussian-Type Basis Sets for Use in Molecular Orbital Studies of Organic Molecules. *J. Chem. Phys.* **1972**, *56*, 2257-2261.

[41] Hariharan, P. C.; Pople, J. A. Influence of polarization functions on molecular-orbital hydrogenation energies. *Theor. Chem. Acc.* **1973**, *28*, 213-222.

[42] Hariharan, P. C.; Pople, J. A. Accuracy of AH equilibrium geometries by single determinant molecular-orbital theory. *Mol. Phys.* **1974**, *27*, 209-214.

[43] Gordon, M. S. The isomers of silacyclopropane. *Chem. Phys. Lett.* **1980**, *76*, 163-168.

[44] Francl, M. M.; Pietro, W. J.; Hehre, W. J.; Binkley, J. S.; DeFrees, D. J.; Pople, J. A.; Gordon, M. S. Self-consistent molecular orbital methods. XXIII. A polarization-type basis set for second-row elements. *J. Chem. Phys.* **1982**, *77*, 3654-3665.

-
- [45] Binning Jr., R. C.; Curtiss, L. A. Compact contracted basis-sets for 3rd-row atoms- Ga-Kr. *J. Comp. Chem.* **1990**, *11*, 1206-1216.
- [46] Blaudeau, J.-P.; McGrath, M. P.; Curtiss, L. A.; Radom, L. Extension of Gaussian-2(G2) theory to molecules containing third-row atoms K and Ca. *J.Chem.Phys.* **1997**, *107*, 5016-5021.
- [47] Rassolov, V. A.; Pople, J. A.; Ratner, M. A.; Windus, T. L. 6-31G* basis set for atoms K through Zn. *J.Chem.Phys.* **1998**, *109*, 1223-1229.
- [48] Rassolov, V.A.; Ratner, M.A.; Pople, J.A.; Redfern, P.C.; Curtiss, L.A. 6-31G* Basis Set for Third-Row Atoms. *J.Comp.Chem.* **2001**, *22*, 976-84.
- [49] Hay, P.J.; Wadt, W.R. *Ab initio* effective core potentials for molecular calculations. Potentials for the transition metal atoms Sc to Hg. *J.Chem.Phys.* **1985**, *82*, 270-283.
- [50] Wadt, W.R.; Hay, P.J. *Ab initio* effective core potentials for molecular calculations. Potentials for main group elements Na to Bi. *J.Chem.Phys.* **1985**, *82*, 284-298.
- [51] Hay, P.J.; Wadt, W.R. *Ab initio* effective core potentials for molecular calculations. Potentials for K to Au including the outermost core orbitals. *J.Chem.Phys.* **1985**, *82*, 299-310.
- [52] Alecu, M.; Zheng, J.; Zhao, Y.; Truhlar, D.G. Computational Thermochemistry: Scale Factor Databases and Scale Factors for Vibrational Frequencies Obtained from Electronic Model Chemistries. *J.Chem. Theory Comput.* **2010**, *6*, 2872-2887.
- [53] McQuarrie, D. A. *Statistical Thermodynamics*, University Science Books, Mill Valley. CA. 1973.
- [54] Foster, J.P.; Weinhold, F. Natural hybrid orbitals *J.Am.Chem.Soc.* **1980**, *102*, 7211-7218.
- [55] Reed, A.E.; Weinhold, F. Natural bond orbital analysis of near-Hartree-Fock water dimer. *J.Chem.Phys.* **1983**, *78*, 4066-4073.
- [56] Reed, A. E.; Weinstock, R. B.; Weinhold. F. Natural population analysis. *J.Chem.Phys.* **1985**, *83*, 735-746.
- [57] Reed, A. E.; Curtiss, L.A.; Weinhold, F. Intermolecular interactions from a natural bond orbital, donor-acceptor viewpoint. *Chem.Rev.* **1988**, *88*, 899-926.

-
- [58] Cretella, D.; Saccani, F.; Quaini, F.; Frati, C.; Lagrasta, C.; Bonelli, M.; Caffarra, C.; Cavazzoni, A.; Fumarola, C.; Galetti, M.; La Monica, S.; Ampollini, L.; Tiseo, M.; Ardizzoni, A.; Petronini, P.G.; Alfieri R.R. Trastuzumab emtansine is active on HER-2 overexpressing NSCLC cell lines and overcomes gefitinib resistance. *Molecular Cancer* **2014**, *13*, 143.
- [59] La Monica, S.; Madeddu, D.; Tiseo, M.; Vivo, V.; Galetti, M.; Cretella, D.; Bonelli, M.; Fumarola, C.; Cavazzoni, A.; Falco A.; Gervasi, A.; Lagrasta, C.A.; Naldi, N.; Barocelli, E.; Ardizzoni, A.; Quaini, F.; Petronini, P.G.; Alfieri, R. Combination of Gefitinib and Pemetrexed Prevents the Acquisition of TKI Resistance in NSCLC Cell Lines Carrying EGFR-Activating Mutation. *J.Thorac.Oncol.* **2016**, doi: 10.1016/j.jtho.2016.03.006.
- [60] Cavazzoni, A.; Alfieri, R.R.; Cretella, D.; Saccani, F.; Ampollini, L.; Galetti, M.; Quaini, F.; Graiani, G.; Madeddu, D.; Mozzoni, P.; Galvani, E.; La Monica, S.; Bonelli, M.; Fumarola, C.; Mutti, A.; Carbognani, P.; Tiseo, M.; Barocelli, E.; Petronini, P.G.; Ardizzoni, A. Combined use of anti-ErbB monoclonal antibodies and erlotinib enhances antibody-dependent cellular cytotoxicity of wild-type erlotinib-sensitive NSCLC cell lines. *Molecular Cancer* **2012**, *11*, 91.
- [61] Fumarola, C.; Caffarra, C.; La Monica, S.; Galetti, M.; Alfieri, R.R.; Cavazzoni, A.; Galvani, E.; Generali, D.; Petronini, P.G.; Bonelli, M.A. Effects of sorafenib on energy metabolism in breast cancer cells: role of AMPK-mTORC1 signaling. *Breast Cancer Res. Treat.* **2013**, *141*, 67–78.
- [62] Rogolino, D.; Bacchi, A.; De Luca, L.; Rispoli, G.; Sechi M.; Stevaert, A.; Naesens, L.; Carcelli, M. Investigation of the salicylaldehyde thiosemicarbazone scaffold for inhibition of influenza virus PA endonuclease. *J.Biol.Inorg.Chem.* **2015**, *20*, 1109-1121.
- [63] Belicchi-Ferrari, M.; Bisceglie, F.; Buschini, A.; Franzoni, S.; Pelosi, G.; Pinelli, S.; Tarasconi, P.; Tavone, M. Synthesis, structural characterization and antiproliferative and toxic bio-activities of copper(II) and nickel(II) citronellal N4-ethylmorpholine thiosemicarbazones. *J.Inorg. Biochem.* **2010**, *104*, 199–206.

-
- [[64] Cowley, A. R.; Dilworth, J. R.; Donnelly, P. S.; White, J. M. Copper complexes of thiosemicarbazone-pyridylhydrazine (THYNIC) hybrid ligands: A new versatile potential bifunctional chelator for copper radiopharmaceuticals. *Inorg. Chem.* **2006**, *45*, 496-498.
- [65] Groom, C. R.; Bruno, I.J.; Lightfoot, M.P.; Ward, S.C. The Cambridge Structural Database. *Acta Cryst.* **2016**, *B72*, 171-179.
- [66] Allen, F. H. The Cambridge Structural Database: a quarter of a million crystal structures and rising *Acta Cryst.* **2002**, *B58*, 380-388.
- [67] Allen, F.H.; Kennard, O.; Watson, D.G.; Brammer, L.; Orpen, A.G. Tables of Bond Lengths determined by X-Ray and Neutron Diffraction. Part 1. Bond Lengths in Organic Compounds. *J. Chem. Soc. Perkin Trans. II* **1987**, S1-S19.
- [68] Wei, L.; Gao, H.; Cui, J. A new 2-((Z)-thiosemicarbazidomethyl)quinolin-8-yl acetate ligand and its Cu(II) complex: syntheses, structures, and characterizations. *Phosphorous, Sulfur, and Silicon* **2012**, *187*, 1101-1108.
- [69] Kurzak, B.; Bogusz, K.; Kroczevska, D.; Jezierska, J. Mixed-ligand copper(II) complexes with diethylenetriamine and histidine- or methionine-hydroxamic acids in water solution. *Polyhedron* **2001**, *20*, 2627-2636.
- [70] Carter, D.C.; Ho, J.X. Structure of serum albumin. *Adv. Protein Chem.* **1994**, *45*, 153-203.
- [71] Rózga, M.; Sokołowska, M.; Protas, A. M.; Bal, W. Human serum albumin coordinates Cu(II) at its N-terminal binding site with 1 pM affinity. *J. Biol. Inorg. Chem.* **2007**, *12*, 913-918.
- [72] Ghuman, J.; Zunszain, P.A.; Petitpas, I.; Bhattacharya, A.A.; Otagiri, M.; Curry, S. Structural Basis of the Drug-binding Specificity of Human Serum Albumin. *J. Mol. Biology* **2005**, *353*, 38-52
- [73] Potůčková, E.; Roh, J.; Macháček, M.; Sahni, S.; Stariat, J.; Šesták, V.; Jansová, H.; Hašková, P.; Jirkovská, A.; Vávrová, K.; Kovaříková, P.; Kalinowski, D.S.; Richardson, D.R.; Šimůnek, T. In Vitro Characterization of the Pharmacological Properties of the Anti-Cancer Chelator, Bp4eT, and Its Phase I Metabolites. *PLoS ONE* **2015**, *10*(10): e0139929.

-
- [74] Markovi, V.; Janicijevi, A.; Stanojkovi, T.; Kolundzija, B.; Sladi, D.; Vujci, M.; Janovi, B.; Joksovi, L.; Djurdjevi, P.T.; Todorovi, N.; Trifunovi, S.; Joksovi, M.D. Synthesis, cytotoxic activity and DNA-interaction studies of novel anthraquinone thiosemicarbazones with tautomerizable methylene group. *Eur.J.Med.Chem.* **2013**, *64*, 228-238.
- [75] Raja, N.; Devika, N.; Gupta, G.; Nayak, V.L.; Kamal, A.; Nagesh, N.; Therrien, B. Biological activities of pyrenyl-derived thiosemicarbazone half-sandwich complexes. *J.Organomet.Chem.* **2015**, *794*, 104-114.
- [76] Lundvig, D.M.; Pennings, S.W.; Brouwer, K.M.; Mtaya-Mlangwa, M.; Mugonzibwa, E.A.; Kuijpers-Jagtman, A.M.; Von den Hoff, J.W.; Wagener, F.A. Curcumin induces differential expression of cytoprotective enzymes but similar apoptotic responses in fibroblasts and myofibroblasts. *Exp.Cell Res.* **2015**, *330*, 429-441.
- [77] Tardito, S.; Barilli, A.; Bassanetti, I.; Tegoni, M.; Bussolati, O.; Franchi-Gazzola, R.; Mucchino, C.; Marchiò, L. Copper-Dependent Cytotoxicity of 8-Hydroxyquinoline Derivatives Correlates with Their Hydrophobicity and Does Not Require Caspase Activation. *J.Med.Chem.* **2012**, *55*, 10448–10459.
- [78] Zhang, Z.; Gou, Y.; Wang, J.; Yang, K.; Qi, J.; Zhou, Z.; Liang, S.; Liang, H.; Yang, F. Four copper(II) compounds synthesized by anion regulation: Structure, anticancer function and anticancer mechanism. *Eur.J.Med.Chem.* **2016**, *121*, 399–409.
- 79 Zeglis, B. M.; Divilov, V.; Lewis, J. S. *J. Med. Chem.* 2011, *54*, 2391
- [80] Stacy, A.E.; Palanimuthu, D.; Bernhardt, P.V.; Kalinowski, D.S.; Jansson, P.J.; Richardson, D.R. Zinc(II)-thiosemicarbazone complexes are localized to the lysosomal compartment where they transmetallate with copper ions to induce cytotoxicity. *J. Med. Chem.* **2016**, *59*, 4965–4984.
- [81] Cavazzoni, A.; Alfieri, R.R.; Carmi, C.; Zuliani, V.; Galetti, M.; Fumarola, C.; Frazzi, R.; Bonelli, M.; Bordini, F.; Lodola, A.; Mor, M.; Petronini, P.G. Dual mechanisms of action of the 5-benzylidene-hydantoin UPR1024 on lung cancer cell lines. *Mol. Cancer. Ther.* **2008**, *7*, 361-370.